

1 **AUG-3387, a Human-Derived Monoclonal Antibody Neutralizes SARS-CoV-2** 2 **Variants and Reduces Viral Load from Therapeutic Treatment of Hamsters** 3 **In Vivo**

4 Christopher J. Emig^{1*}, Marco A. Mena¹, Steven J. Henry¹, Adela Vitug¹, Christian John Ventura¹, Douglas Fox², Xammy
5 Huu Nguyen³, Haiyue Xu⁴, Chaeho Moon⁴, Sawittree Sahakijjijarn⁵, Philip J. Kuehl⁶, David Revelli⁶, Zengrong Cui⁴,
6 Robert O. Williams III⁴, and Dale J. Christensen^{5*}

7 ¹Augmenta Bioworks, 3475 Edison Way, Suite K, Menlo Park, CA 94025 USA

8 ²School of Public Health, Division of Infectious Diseases and Vaccinology, University of California, Berkeley, 1951 Oxford Street, Berkeley, CA 94720

9 ³Department of Molecular and Cellular Biology, University of California, Berkeley, 1951 Oxford Street, Berkeley, CA 94720

10 ⁴Molecular Pharmaceutics and Drug Delivery Division, College of Pharmacy, The University of Texas at Austin, 2409 University Avenue, Austin, TX, 78712,
11 USA

12 ⁵TFF Pharmaceuticals, Inc., Austin, TX, 78746 USA

13 ⁶Lovelace Biomedical Research Institute, Albuquerque, NM 87108, USA

14 * Correspondence:

15 **Abstract**

16 Infections from the SARS-CoV-2 virus have killed over 4.6 million people since it began spreading
17 through human populations in late 2019. In order to develop a therapeutic or prophylactic antibody
18 to help mitigate the effects of the pandemic, a human monoclonal antibody (mAb) that binds to the
19 SARS-CoV-2 spike protein was isolated from a convalescent patient following recovery from COVID-
20 19 disease. This mAb, designated AUG-3387, demonstrates a high affinity for the spike protein of
21 the original viral strains and all variants tested to date. *In vitro* pseudovirus neutralization and SARS-
22 CoV-2 neutralization activity has been demonstrated in vitro. In addition, a dry powder formulation
23 has been prepared using a Thin-Film Freezing (TFF) process that exhibited a fine particle fraction
24 (FPF) of $50.95 \pm 7.69\%$ and a mass median aerodynamic diameter (MMAD) and geometric standard
25 deviation (GSD) of $3.74 \pm 0.73 \mu\text{m}$ and 2.73 ± 0.20 , respectively. The dry powder is suitable for
26 delivery directly to the lungs of infected patients using a dry powder inhaler device. Importantly,
27 AUG-3387, administered as a liquid by intraperitoneal injection or the dry powder formulation
28 delivered intratracheally into Syrian hamsters 24 hours after intranasal SARS-CoV-2 infection,

29 demonstrated a dose-dependent reduction in the lung viral load of the virus. These data suggest
30 that AUG-3387 formulated as a dry powder demonstrates potential to treat COVID-19.

31 **Keywords**

32 Pulmonary administration; Thin-Film Freezing; monoclonal antibody; Dry powder inhaler; SARS-
33 CoV-2 therapy, hamster model

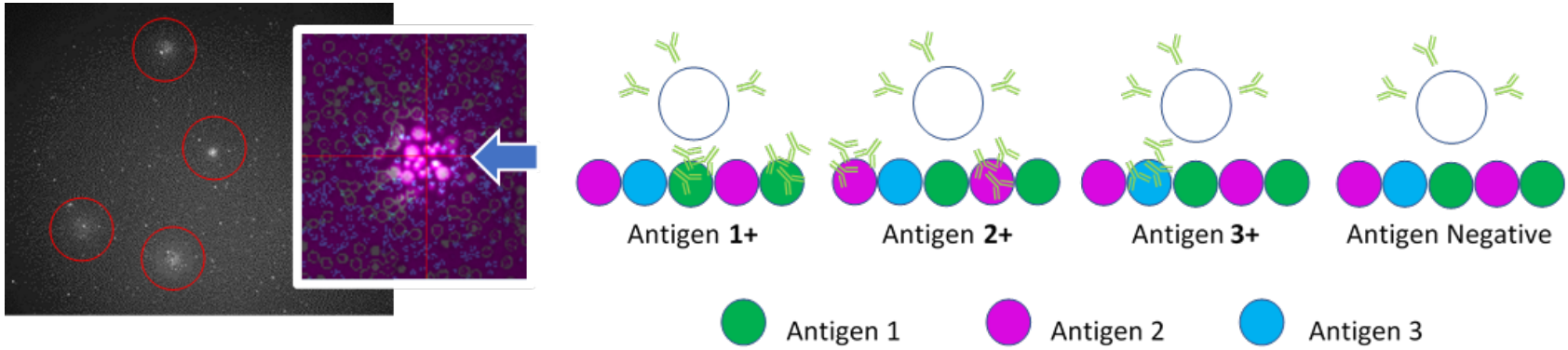
34 **1. Introduction**

35 Infections caused by a novel coronavirus began emerging in late 2019 that became known as the
36 Severe Acute Respiratory Syndrome Coronavirus 2 (SARS-CoV-2) virus. This Coronavirus Disease
37 2019 (COVID-19) pandemic has resulted in the loss of more than 4.6 million lives globally to date.
38 The SARS-CoV-2 virus is related to the etiological agents causing the SARS epidemic in 2002-2003
39 and the Middle East Respiratory Syndrome (MERS) epidemic of 2012 (1, 2). The COVID-19 pandemic
40 has resulted in more deaths than any other recent epidemics (1, 3, 4) and has had profound effects
41 on the lives of people around the world. One key mitigation strategy employs neutralizing
42 monoclonal antibodies (mAbs) to treat or protect against SARS-CoV-2 infection. Since the outbreak,
43 multiple mAb products have been granted Emergency Use Authorization (EUA) but all are
44 administered by infusion or injection. These include Casirivimab and Imdevimab produced by
45 Regeneron, Bamlanivimab and Etesevimab marketed by Lilly, and Sotrovimab from Glaxo Smith
46 Klein in partnership with Vir Biologics. Although generally limited to infusion centers and out-patient
47 settings, mAb therapies have proven to reduce hospitalization in mild to moderate COVID-19
48 patients.

49 Routes for discovery of new SARS-CoV-2 neutralizing antibodies include isolation of antibody
50 sequences from patients who have recovered from SARS-CoV-2 or SARS-CoV-1, inoculation and

51 isolation of humanized mice, or the use of phage or other library display technology. Over the past
52 two decades, several groups have published methods for isolating, sequencing and cloning antibody
53 genes from single B cells from primary patient samples, then expressing antibody protein for
54 characterization (5-7). We have developed workflows for discovery of antigen specific membrane
55 bound antibodies via cytometry, and secreted antigen-specific antibodies via our proprietary
56 SingleCyte[®] instrument (Augmenta Bioworks). SingleCyte[®] is a motorized microscope with an
57 intelligent image processing engine driving a single cell retrieval device. A typical SingleCyte[®] assay
58 measures antigen binding of secreted antibodies against 4 antigen targets for up to 240,000 single
59 cells in a standard SBS format plate and retrieves approximately 200 antigen specific single B cells
60 (Figure 1). Single cells isolated using SingleCyte or FACS are deposited into 96 well plates and heavy
61 and light chain mRNAs are reverse transcribed, amplified and sequenced. The sequences are then
62 PCR amplified or synthesized and cloned into expression vectors. We have developed a fully
63 integrated and highly automated platform for performing these workflows in under ten days and
64 have had previous success in identifying antibodies targeting other infectious disease antigens,
65 including herpes simplex virus and influenza virus.

66 Since SARS-CoV-2 is primarily a pulmonary disease, early treatment or prophylaxis with neutralizing
67 mAb therapy targeted to the airways could improve disease outcomes. Initiating treatment early in
68 the disease cycle may alter the course of the disease, prevent the development of chronic
69 complications, reduce the hospitalization rate and decrease mortality. Only a fraction of a
70 systemically administered mAb is transported into the pulmonary compartment where viral
71 particles are released early in the disease; therefore, delivery of neutralizing mAbs directly to the
72 lung holds the potential to reduce the dose needed to achieve the same efficacy as systemically
73 delivered mAbs. Aerosolized delivery would have additional benefits including the potential for
74 patients to self-administer antibody therapy at home rather than in infusion centers, and the ability



75

76 **Figure 1. Illustration of the SingleCyte[®] cell isolation process.** Cells are assayed for their ability to secrete proteins that bind various optically
 77 encoded antigens in their proximity and target cells are selected and isolated using an automated system.

78

79

80 to expand the supply of antibody to treat a larger population through dose-reduction. Furthermore,
81 a dry antibody formulation stable at ambient temperatures could be made available to patients in
82 geographic regions that lack suitable infrastructure for cold chain distribution of injectible antibody
83 formulations that require cold chain distribution.

84 Thin-film freezing (TFF) is a particle engineering technology that has been used to prepare dry
85 powder formulations of drugs that are administered to patients using a dry powder inhaler (DPI)
86 device. Powders produced by this process are currently in human clinical testing for the treatment
87 of pulmonary indications (NCT04872231 and NCT04576325) (8, 9) and have characteristic highly
88 porous brittle matrices with low bulk densities that can be delivered with good aerosol performance
89 (10). The TFF technology generates these powders by fast supercooling of drug-carrier solutions (11)
90 followed by lyophilization to remove water or other solvents and has been used to generate
91 powders of small molecule (12, 13) and biologic drugs (14).

92 We now report the isolation of a fully human mAb, AUG-3387, using the SingleCyte® system, which
93 binds to the SARS-CoV-2 spike protein with high affinity and binds to all SARS-CoV-2 variant spike
94 proteins tested to date including Delta, Lamda and Mu. In vitro neutralization was confirmed using
95 pseudovirus neutralization with the wild-type SARS-CoV-2 and the Delta variant (B.1.617.2) spike
96 protein pseudotyped lentivirus. Direct neutralization of wild-type SARS-CoV-2 was also
97 demonstrated in vitro where AUG-3387 demonstrated a 99.99% reduction of infection of VERO-E6
98 cells at therapeutically relevant doses, which demonstrated that AUG-3387 has potential to treat or
99 prevent COVID-19 disease. In order to translate these findings to prepare for clinical trials, AUG-
100 3387 was formulated into a dry powder formulation that is stable at ambient temperatures using
101 the Thin Film Freezing process as a powder that contains 15% weight to weight of the antibody. The
102 dry powder was delivered to Syrian golden hamsters in an in vivo therapeutic model of COVID-19
103 disease where treatment with AUG-3387 was initiated 24 hr after inoculation with SARS-CoV-2. In

104 this model, three daily intratracheal insufflation administrations of the dry powder or a single
105 intraperitoneal injection of AUG-3387 in liquid formulation demonstrated a dose-responsive
106 reduction in viral titer in lung tissue at day 5. Taken together, these data demonstrate the potential
107 for AUG-3387 to treat or prevent COVID-19.

108 2. Materials and Methods

109 2.1. Materials

110 The reagents and suppliers listed in Table 1 were used to complete the studies.

111 **Table 1: Reagents and Supplies**

Reagent	Supplier	Catalog Number
SARS-CoV-2 Wuhan-1 RBD	Sino Biological	40592-V08B
B.1.1.17 (Alpha) S1	Sino Biological	40591-V08H12
20H/501Y.V2 (Beta) S1	Sino Biological	40591-V08H10
B.1.617.2 (Delta) RBD	Sino Biological	40592-V08H86
B.1.1.28 (Gamma) S1+S2	Sino Biological	40589-V08B10
B.1.617 (Kappa) RBD	Sino Biological	40592-V08H88
SARS-CoV-2 S494P RBD	Sino Biological	40592-v08h18
SARS-CoV-2 V483A RBD	Sino Biological	40592-v08h5
SARS-CoV-2 R683A, R685A, F817P, A892P, A899P, A942P, K986P, V987P S1+S2	Sino Biological	40589-v08h4
SARS-CoV-2 G485S RBD	Sino Biological	40592-v08h52
SARS-CoV-2 D614G,E484K S1	The Native Antigen Company	REC31902
SARS-CoV-2 D614G, V445I, H655Y, E583D S1	The Native Antigen Company	REC31903

SARS-CoV-2 Spike-E-M Mosaic Protein	The Native Antigen Company	REC31829-100
SARS-CoV-2 (2019-nCoV) Spike Protein (S2 ECD, His tag)	Sino Biological	40590-V08B
SARS-CoV-2 Spike Glycoprotein (S1) "Supplier 2"	The Native Antigen Company	REC31828-100
SARS-CoV-2 (2019-nCoV) Spike Protein (S1+S2 ECD, His tag)	Sino Biological	40589-V08B1
SARS-CoV-2 (2019-nCoV) Spike Protein (S1 Subunit, His Tag) "Supplier 1"	Sino Biological	40591-V08H
SARS-CoV-2 L452R,T478K RBD	Sino Biological	40592-V08H90
SARS-CoV-2 Lenti Pseudovirus	GenScript	SC1993-2
SARS-CoV-2 Delta Lenti Pseudovirus	e-Enzyme	SCV2-PsV-Delta
BSA	ROCKLAND IMMUNOCHEMICALS	BSA-50
HEK293T	ATCC	CRL-3216
pCMV-AC-GFP Ace2 Expression Vector	Origene	pCMV-AC-GFP
ACE2 Polyclonal antibody	ProteinTech	21115-1-AP
PE Donkey anti-rabbit IgG	BioLegend	406421
MagPlex -C Microspheres	Luminex	MC10012-01, etc (various)
Antibody Conjugation Kit	Luminex	40-50016
Thermo Scientific Zeba Spin Desalting Columns, 7K MWCO, 0.5 mL	Thermo Scientific	PI89883
1 xMAP Sheath Fluid, 20L, RUO	Luminex	40-50015
PE anti-human IgG/IgA/IgM	Sigma	AQ503H
Thermo Scientific Zeba Spin Desalting Columns, 7K MWCO, 0.5 mL	Thermo Scientific	PI89883
Anti-V5 antibody clone SV5-Pk1	Abcam	ab27671
BrightGlo Luciferase Reagent	Promega	E2620

113 **2.2. Antibody Isolation**

114 For this study, we profiled patients with low disease burden, rather than severely affected
115 individuals. We hypothesized that asymptomatic or weakly symptomatic patients might have had
116 previous exposure to a related antigen (e.g., other coronaviruses), providing a breadth of antigenic
117 coverage and driving their resistance to COVID-19. Informed consent was obtained from all patients,
118 and all patient samples were collected after a full recovery from illness and under IRB approval.
119 Patient samples were profiled to identify samples with binding to multiple SARS-CoV-2 proteins
120 including the S1-receptor binding domain (RBD), full length S1, S2, E and M protein. From each
121 sample, plasma was separated from PBMC's and red blood cells by Ficoll density gradient
122 centrifugation (Cytiva). Additionally, approximately 100k B cells were extracted from whole blood
123 (RosetteSep, StemCell) and seeded directly, or terminally differentiated into plasma cells and then
124 seeded into SingleCyte[®] assay plates with up to 4 different optically encoded SARS-CoV-2 antigens
125 or controls. A fluorescently labelled anti-human IgG/IgA/IgM secondary antibody was also added
126 to each well. After a 24 hour incubation, antigen specific cells were identified by their signature
127 reaction-diffusion pattern. For identification of surface bound antibodies binding to SARS-CoV-2,
128 SARS-CoV-2 antigens conjugated to Alexa Fluor 488 stained SARS-CoV-2 antigen was used as a
129 staining agent for single cell sorting of antigen reactive memory B cells into 96 well plates on a Sony
130 SH-800 Cell Sorter. Cells specific to any SARS-CoV or SARS-CoV-2 antigen were retrieved and
131 sequenced.

132 The sequences were analyzed for unique clonotypes based on CDR3 sequences of heavy and light
133 chains, then unique clonotypes were designed into DNA fragments for cloning through Augmenta's
134 AbWorks[™] automated clone design software. The fragments were cloned as ScFv's for expression
135 in E. coli, or as full heavy and light chains in mammalian expression vectors for tandem transfection
136 into Expi293T.

137 SingleCyte® is Augmenta’s programmable single cell imaging cytometer and sorter that selects cells
138 based on temporal microscopy. For screening of secreted antibody proteins, assay plates contain a
139 multiplexed panel of antigens in the form of conjugated beads or antigen presenting cells and a
140 secondary antibody in solution. Antibodies from secreted cells bind proximal antigens and become
141 physically constrained near the secreting cell. Fluorescent secondary antibody enables visualization
142 of secreted antibody concentration gradients based on fluorescence over time, and optically
143 encoded antigen beads enables deconvolution of target antigens. Assays are performed in standard
144 open well SBS footprint microplates and are user programmable. The instrument works by first
145 raster imaging each well. Cells with any antigen reactivity are identified by processing images with
146 a convolutional neural network trained on a set of manually curated images. The microscope
147 performs multispectral high resolution imaging of each positive cell. Images are masked into regions
148 by the optical characteristics of proximal beads and a confidence score is ascribed to each cell-
149 antigen interaction. Single cells are then picked and placed into receiver plates and post-isolation
150 images are taken to ensure proper aspiration of target cells. A robotic arm carries receiver plates
151 for high throughput single cell retrieval. The information for each run and output metrics for each
152 cell (including both source and destination locations) are saved to a database for recall in a user
153 interface and for downstream processing steps.

154 **2.3. Antibody Chracterization**

155 2.3.1 Target Binding Characterization

156 SARS-CoV-2 S1 and RBD proteins, and various other antigens and controls, were covalently coupled
157 to Luminex MagPlex magnetic microspheres for assay binding with a Luminex 200 instrument. The
158 following antigens were conjugated: B.1.1.17 (Alpha) S1, B.1.1.28 (Gamma) S1+S2, 20H/501Y.V2
159 (Beta) S1, B.1.617 (Kappa) RBD, B.1.617.2 (Delta) RBD, S1+S2 S494P, S1+S2 V483A, S1+S2

160 R683A+R685A+F817P+A892P+A899P+A942P+ K986P+V987P, S1+S2 G485S, S1+S2 D614G, S1+S2
161 E484K, S1+S2 D614G+V445I+H655Y+E583D, S1+S2 L452R+T478K. Each antigen was conjugated with
162 the xMAP conjugation kit at ratio of 5µg protein to 1 million beads. Assays were performed in
163 multiplex, with each spectrally encoded bead having a separate antigen and run together in a single
164 well. Antibody was titrated over therapeutically relevant concentrations, mixed with the beads,
165 washed twice, labelled with a secondary antibody, washed twice and run on the instrument. Dry
166 powder versions of antibodies were resuspended in water before dilution for assay.

167 The ScFv version of AUG-3387, designated AUG-3705, was run on a Cytex LSA instrument at
168 multiple concentrations for determination of the single domain affinity against Wuhan SARS-CoV-2
169 S1 and RBD. AUG-3705 was attached to the LSA flow cell via interaction with its V5 tag and a surface
170 bound anti-V5 antibody. Wuhan-1 RBD was delivered to the flow cell at concentrations of 2.06nM,
171 6.17nM, 18.5nM and 56nM for calculation of Kd.

172 **2.4. Pseudoneutralization Assay**

173 **2.4.1 ACE-2 Expressing HEK293T Cell Line Construction**

174 An ACE2 expressing HEK293T cell line (“LentiX ACE2.S4”) was constructed by packaging pCMV-AC-
175 GFP (Origene) into lentivirus and transducing HEK293T’s (ATCC). The cells were enriched 4 times
176 until 97% of the cells showed signal above the negative control as read out by staining with anti-
177 ACE-2 and secondary antibodies. On average enriched ACE2-HEK293T’s had 50-fold higher signal
178 compared to the signal of non-transduced cells.

179 **2.4.2 SARS-CoV-2 Pseudovirus with TFF powder formulation and soluble AUG-3387**

180 Two days prior to infection, LentiX ACE2.S4 cells were grown to 85% confluency, then seeded in a
181 96-well plate at 15k cells/well in 50µL media per well and held at 37 °C in 5% CO₂ until infection.
182 Antibody mixes were created prior to infection by performing a 128-fold serial dilution starting at

183 40µg/µL. Dry powders prepared by the TFF process of AUG-3387 and soluble negative control V5
184 Tag monoclonal antibody were seeded in triplicate, and soluble AUG-3387 was seeded in duplicate.
185 SARS-CoV-2 pseudovirus (Genscript) was diluted in DMEM complete media to an IFU of 3.2e7/mL,
186 and 100µL of virus solution was mixed with 100 µL of diluted antibody. The virus/antibody mix was
187 incubated for 60 minutes at 37 °C in 5% CO₂. Following incubation, 50 µL of each
188 pseudovirus/antibody condition mix was added to each well of seeded cells. Additional controls
189 included cells only, and cells with virus only. After 48 hours, the plate was removed and equilibrated
190 at room temperature for 10 minutes, and 60 µL of the supernatant was removed. 50 µL of Promega's
191 Bright-Glo Luciferase assay reagent was added to each well of the infected cells. The cells then were
192 incubated at room temperature for 3 minutes, and luminescence was measured with a Tecan Spark
193 microplate reader with a 1 second integration time.

194 **2.4.3 SARS-CoV-2 Pseudovirus, Delta Variant (B.1.617.2) with soluble AUG-3387**

195 Two days prior to infection, LentiX ACE2.S4 cells were grown to 85% confluency, then seeded in a
196 96-well plate at 15k cells/well in 50µL media per well and held at 37 °C in 5% CO₂ until infection.
197 Antibody mixes were created prior to infection by performing a 128-fold serial dilution starting at
198 160µg/µL. AUG-3387 and negative control V5 Tag monoclonal antibody were seeded in triplicate.
199 SARS-CoV-2 Delta Variant pseudovirus (eEnzyme) was diluted 1:2 in DMEM complete media to a
200 pseudoviral particle concentration of 5e7/ml, and 200µL of virus solution was mixed with 200µL of
201 diluted antibody. The virus/antibody mix was incubated for 60 minutes at 37 °C in 5% CO₂. Following
202 incubation, 100µL of each pseudovirus/antibody condition mix was added to each well of seeded
203 cells. Additional controls included cells only, and cells with virus only. After 48 hours, the plate was
204 removed and equilibrated at room temperature for 10 minutes, and 100µL of the supernatant was
205 removed. 50µL of Promega's Bright-Glo Luciferase assay reagent was added to each well of the

206 infected cells. The cells then were incubated at room temperature for 3 minutes, and luminescence
207 was measured with a Tecan Spark microplate reader with a 1 second integration time.

208 **2.5. SARS-CoV-2 Neutralization Assay**

209 Two days prior to infection, Calu-3 cells were grown to confluency, then seeded at 40k cells in 100 μ L
210 media per well. Antibody was titrated in D10 media. The reagents were then transferred into a Bio
211 Safety Level 3 facility for further processing. For each antibody condition, SARS-CoV-2 virus at a
212 target MOI of 0.05 was mixed with antibody at the desired concentration and incubated at 37 °C for
213 60 minutes. Media was removed from the seeded cells and replaced with a final volume of 50 μ L of
214 antibody/virus mix. Cells with antibody and virus (MOI 0.05) were incubated at 37 °C in 5 % CO₂ for
215 30 minutes. The virus/antibody mix was removed and the cells were washed with 75 μ L PBS. Cells
216 were replenished with titrated antibody in a final volume of 150 μ L media.

217 After 24 hours, 50 μ L of the supernatant was removed for TCID₅₀ assays. Vero E6 cells were seeded
218 at 10,000 cells in 100 μ L per well. Infected cell culture supernatant was diluted with 950 μ L D10
219 media, and then serial diluted before 50 μ L of each dilution was added to 8 wells of Vero E6 cells.
220 After 72 hours, wells with complete cytopathic effect were counted. After 96 hours, 100 μ L
221 CellTiterGlo reagent was added to each well of the infected Calu-3 cells to assay for live cells.
222 Following incubation of CTG reagent for 20 minutes, luminescence was measured with a Spectramax
223 1L with 1s integration time.

224 **2.6. Preparation of Thin Film Freezing (TFF) composition**

225 In the preparation of the solutions for TFF manufacturing, AUG-3387 was combined with a
226 mannitol/leucine or trehalose/leucine. The solution was applied as drops onto a rotating
227 cryogenically cooled drum cooled to -70 °C. The frozen solids were collected and stored in a -80 °C
228 freezer before lyophilization. The lyophilization was performed in an SP VirTis Advantage Pro shelf

229 lyophilizer (SP Industries, Inc., Warminster, PA, USA). The primary drying process was at -40°C for
230 20 h, and then, the temperature was linearly increased to 25°C over 20 h, followed by secondary
231 drying at 25°C for 20 h. The pressure was maintained at less than 100 mTorr during the lyophilization
232 process.

233 **2.7. Aerodynamic particle size distribution analysis**

234 About three milligrams of AUG-3387 mAb dry powder was loaded into size #3 hydroxypropyl
235 methylcellulose (HPMC) capsules (Vcaps[®] plus, Capsugel[®], Lonza, Morristown, NJ, USA). The
236 aerodynamic properties of the powder were evaluated using a Next Generation Impactor (NGI)
237 (MSP Corporation, Shoreview, MN, USA) connected to a High-Capacity Pump (model HCP5, Copley
238 Scientific, Nottingham, UK) and a Critical Flow Controller (model TPK 2000, Copley Scientific,
239 Nottingham, UK). A high-resistance Plastiap[®] RS00 inhaler (Plastiap S.p.A, Osnago, Italy) was used
240 for dispersing the powder through the USP induction port with a total flow rate of 60 L/min for 4 s
241 per each actuation corresponding to a 4 kPa pressure drop across the device and a total flow volume
242 of 4 L. To avoid particle bounce, a solution of polysorbate 20 in methanol at 1.5% (w/v) was applied
243 and dried onto the NGI collection plates to coat their surface. The pre-separator was not used in this
244 analysis. After dispersal, the powder was extracted from the stages using water.

245 Quantitation of mannitol or trehalose recovered from NGI stages was performed on an Agilent 1220
246 Infinity II HPLC system (Santa Clara, CA) with a Waters XBridge Amide column (4.6 x 150 mm, 3.5
247 μm) (Milford, MA) connected to Agilent 1290 Infinity II ELSD (Santa Clara, CA). A gradient method
248 with mobile phase B, from 80% to 40% acetonitrile with 0.1 % (v/v) trifluoroacetic acid, and mobile
249 phase A, water, was used at the mobile phase flow rate of 1.0 mL/min and the column temperature
250 of 30°C . 15 μL of each sample was injected and ran for 6 minutes. Evaporative and nebulizer
251 temperatures of ELSD were set at 60°C , and the gas (dry nitrogen) flow rate was 1.6 L/min.

252 The analysis was conducted three times (n=3). The NGI results were analyzed using the Copley
253 Inhaler Testing Data Analysis Software 3.10 (CITDAS) (Copley Scientific, Nottingham, UK). CITDAS
254 provided the calculation for mass median aerodynamic diameter (MMAD), geometric standard
255 deviation (GSD), fine particle fraction (FPF) of delivered dose (FPF%, delivered) and recovered dose
256 (FPF%, recovered). The FPF of delivered dose was calculated as the total amount of sugar or sugar
257 alcohol (e.g., trehalose, mannitol) collected with an aerodynamic diameter below 5 μm as a
258 percentage of the total amount of sugar or sugar alcohol deposited on the adapter, the induction
259 port, stages 1–7 and Micro-Orifice Collector.

260 **2.8. Efficacy of AUG-3387 in and in vivo model of SARS-CoV-2 infected Syrian Hamsters**

261 An *in vivo* efficacy study was performed with male Syrian Hamsters (*Mesocricetus auratus*)
262 approximately 9 weeks of age with a weight range of 110-134 g, at time of randomization, were
263 sourced from Charles River Laboratory. Animal work was performed at Lovelace Biomedical
264 Research Institute (LBRI), with approval from the Institutional Animal Care and Use Committee
265 (IACUC) and within Animal Biosafety Level 3 (ABSL3) containment. Hamsters were singly housed in
266 filter-topped cage systems and were supplied with a certified diet, filtered municipal water, and
267 dietary and environmental enrichment. The challenge study design is detailed in Table 2. Animals
268 were assigned to groups using a stratified (body weight) randomization procedure. Animals were
269 anesthetized and swabs of nasal passages were collected by placing the nasal swab (0.5 mm
270 diameter Ultrafine Micro Plasdent swabs) 1-3 mm into the nares and swabbing. Lung and nasal swab
271 (in Trizol) samples were stored at -80°C prior to analysis. All animals were euthanized with an
272 euthanasia solution consisting of 390 mg of sodium pentobarbital and 50 mg of phenytoin per mL.

273

Table 2: Group Designations of animals in the efficacy study

Group	Group Description	Challenge Day	Dose	Route/Frequency	Number of animals	Study Endpoints
1	Vehicle Control	Day 0	0.0	IP; once on Day 1	6	Daily Clinical Observations Twice Daily Body Weights Daily Nasal swabs on Days 1 and 5 for viral load Necropsy on day 5 for viral load of lung tissue and Histopathology of lungs
2	mAb-1 High dose	Day 0	1.0 mg/kg	IT; once daily on Days 1,2,3	6	
3	mAb-1 Low dose	Day 0	0.33 mg/kg	IT; once daily on Days 1,2,3	6	
4	mAb-solution High dose	Day 0	10.0 mg/kg	IP; once on Day 1	6	
5	mAb-solution Low dose	Day 0	3.3 mg/kg	IP; once on Day 1	6	

274

275 **2.8.1 Viral Challenge**

276 SARS-CoV-2, isolate USA-WA1/2020, was sourced from WRCEVA and propagated in Vero E6 African
277 Green Monkey kidney cells (BEI, catalog #N596) in Dulbecco's Modified Eagle Medium
278 supplemented with 1% HEPES, 10% FBS, 100 IU/mL Penicillin G and 100 µg/mL Streptomycin. Stocks
279 were stored in a BSL-3 compliant facility at -80°C prior to challenge. Stock vials of virus were thawed
280 the day of challenge, diluted as necessary, and stored on wet ice until use. Viral challenge dose was
281 quantitated using a Tissue Culture Infectious Dose 50% (TCID₅₀) assay using the Reed and Muench
282 method (15) on Vero E6 cells in DMEM supplemented with 2% FBS and 100 IU/mL Penicillin G and
283 100 µg/mL Streptomycin. A challenge dose of 1.0×10^5 TCID₅₀ per animal was targeted. Actual
284 challenge dose averaged 5.8×10^5 TCID₅₀ per animal. The viral challenge dose was delivered via
285 intranasal installation under anaesthesia (ketamine 80 mg per kg and xylazine 5 mg per kg) with a
286 volume of 100 µL per nare (200 µL total per animal).

287 **2.8.2 AUG-3387 Treatment**

288 The AUG-3387 mAb was delivered by one of two routes for each animal, IT and IP injection. The IP
289 injection was performed with a 16 mg/mL formulation in saline. Intratracheal insufflation was
290 performed with animals under anesthesia (4-5% isoflurane with oxygen) until a deep plane of
291 anesthesia was reached. Dry powder for inhalation delivery was transferred to the ABSL-3 facility
292 and each individual device quantitatively loaded for delivery. Doses were based on method
293 development to quantify the amount of material that exited the devices assuming 100%
294 presentation at the terminus of the canule and the animals average body weight during dosing.

295 **2.8.3 Quantitative Assessment of Viral Burden**

296 Quantitation of genomic viral RNA and subgenomic viral RNA, by RT-qPCR was used as markers for
297 viral burden. Nasal swab and lung samples were assayed via RT-qPCR for both the N-gene (genomic)
298 and the E-gene (subgenomic). For both methods, lung samples were weighed and homogenized
299 using a Tissue Lyser (Qiagen) in 1 ml of TRI reagent. RNA was extracted using the Direct-Zol 96- RNA
300 kit (Zymo Research) according to manufacturer's instructions. RNA was quantified using qRT-PCR
301 TaqMan Fast Virus 1-step assay (Applied Biosystems). SARS-CoV-2 specific primers and probes from
302 the 2019-nCoV RUO Assay kit (Integrated DNA Technologies) were used: (L
303 Primer:TTACAAACATTGGCCGCAAA; R primer: GCGCGACATTCCGAAGAA; probe: 6FAM-
304 ACAATTTGCCCCAGCGCTTCAG-BHQ-1). Reactions were carried out on a BioRad CFX384 Touch
305 instrument according to the manufacturer's specifications. A semi-logarithmic standard curve of
306 synthesized SARS-CoV-2 N gene RNA (LBRI) was obtained by plotting the Ct values against the
307 logarithm of cDNA concentration and used to calculate SARS-CoV-2 N gene in copies per gram of
308 tissue or per nasal swab.

309 Copies of SARS-CoV-2 E gene were measured by qRT-PCR TaqMan Fast Virus 1-step assay (Thermo
310 Fisher). SARS-CoV-2 specific primers and probes from the 2019-nCoV RUO Assay kit (Integrated DNA

311 Technologies) were used: (L Primer: CGATCTCTGTAGATCTGTTCTC; R primer:
312 ATATTGCAGCAGTACGCACACA; probe: 6FAM-ACACTAGCCATCCTTACTGCGCTTCG-BHQ-1). Reactions
313 were carried out on a BioRad CFX384 Touch instrument according to the manufacturer's
314 specifications. A semi-logarithmic standard curve of synthesized SARS-CoV-2 E gene RNA (LBRI) was
315 obtained by plotting the Ct values against the logarithm of cDNA concentration and used to calculate
316 SARS-CoV-2 E gene in copies per gram of tissue or per nasal swab. Thermal cycling conditions
317 involved 5 minutes at 50°C for reverse transcription, followed by an initial denaturation step for 20
318 seconds at 95°C and 40 cycles of 95°C for 3 seconds and 60°C for 30 seconds.

319 3. Results and Discussion

320 **3.1. Antibody Isolation**

321 In order to isolate antibodies that bind and neutralize SARS-CoV-2, samples from seven study
322 subjects were profiled for the presence of SARS-CoV-2 antibodies using a Luminex-based profiling
323 6-fold multiplex assay (Supplemental Figure 1). A proprietary instrumentation platform known as
324 SingleCyte[®] was used to select SARS-CoV-2-reactive antibody-producing B-cells. SingleCyte[®] is a
325 programmable single cell imaging cytometer and sorter that selects cells based on temporal
326 microscopy. For screening of secreted antibody proteins, assay plates contain a multiplexed panel
327 of antigens in the form of conjugated beads or antigen presenting cells and a secondary antibody in
328 solution. Antibodies from secreted cells bind proximal antigens and become physically constrained
329 near the secreting cell. Fluorescent secondary antibody enables visualization of secreted antibody
330 concentration gradients based on fluorescence over time, and optically encoded antigen beads
331 enables deconvolution of target antigens (Figure 2a). Assays are performed in standard open well
332 SBS footprint microplates and are user programmable. A custom nanoliter volume micropipette

333 enables isolation of single cells, and a robotic arm carries receiver plates for high throughput single
334 cell retrieval.

335 Approximately 800 single cells were isolated with SingleCyte and 200 with single cell flow sorting.
336 From these cells, nearly 500 paired chain antibody constructs were designed and approximately 200
337 were expressed and assayed (Figure 2b). We recovered many S1, S2, and RBD binders and ultimately
338 chose AUG-3387 as our lead compound due to its breadth of binding activity, affinity to the Wuhan-
339 1 strain, and strength in viral neutralization. The timeline for isolation process is shown in
340 Supplemental Figure 2.

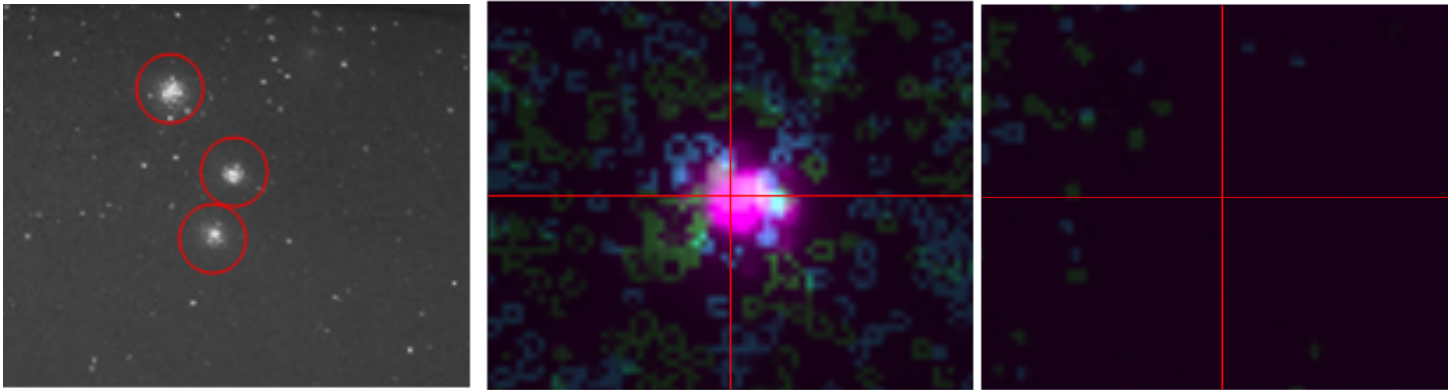
341 **3.2. Antibody Characterization**

342 **3.2.1 AUG-3387 Single Domain Affinity**

343 We utilized the Carterra LSA platform to determine the single domain affinity of AUG-3387
344 expressed as an ScFv, designated AUG-3705. Auto-fitting of curves was performed in Carterra
345 Kinetics software, which returned a calculated affinity of 1.2 nM (Fig 3).

346

A)

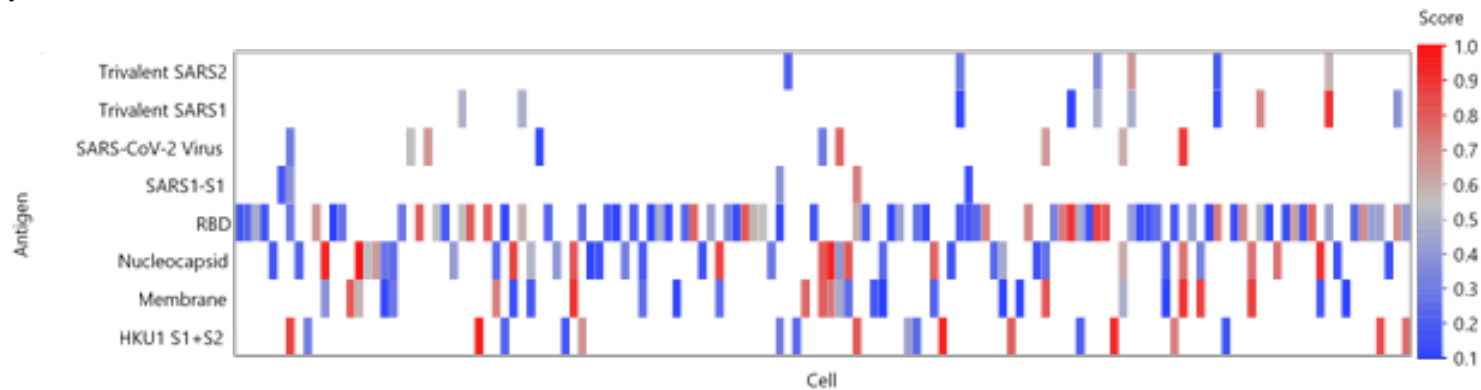


347

348

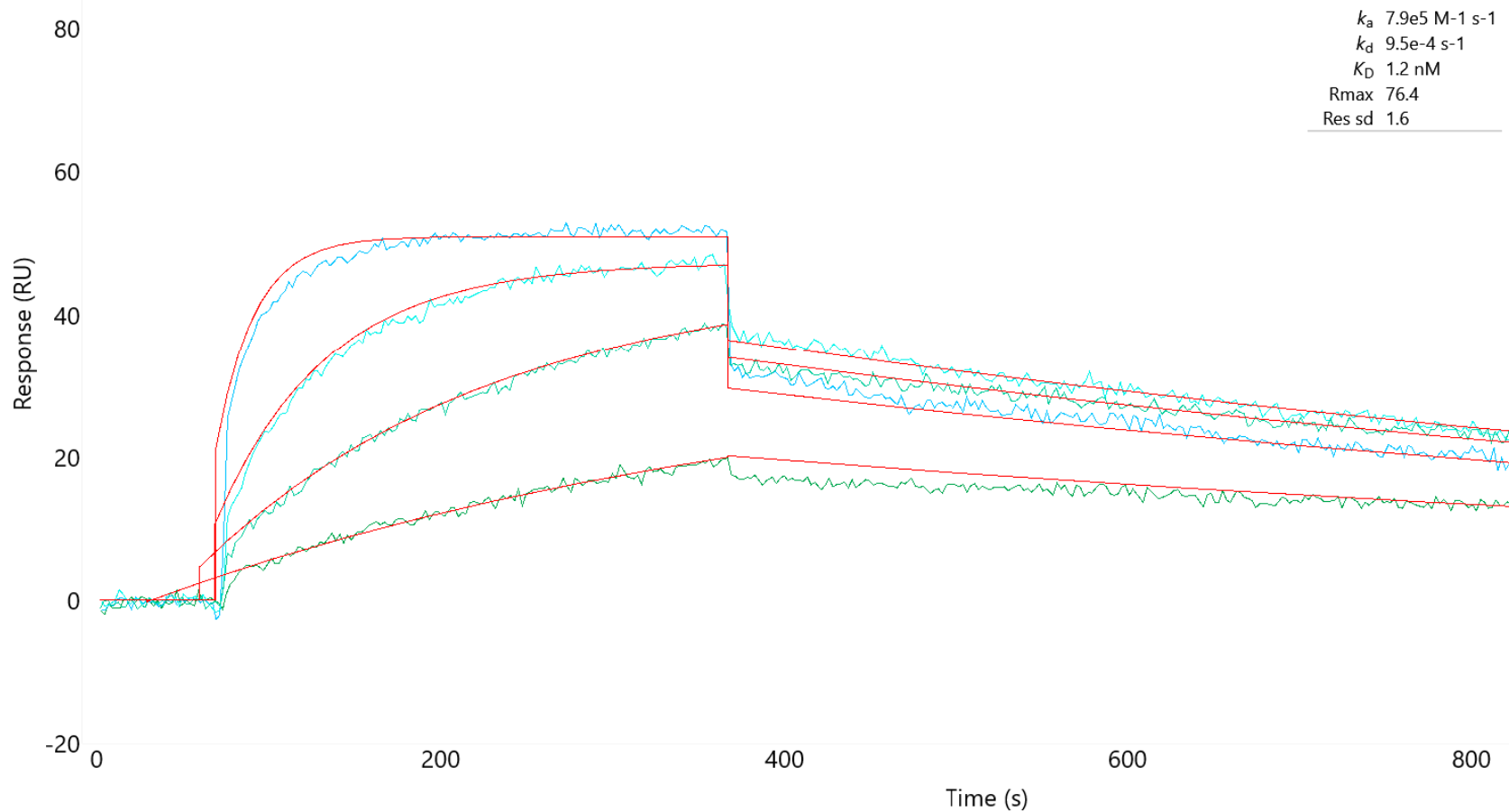
349

B)



350

351 **Figure 2: Isolation and Characterization of SARS-CoV-2 binding Cells:** A) Raster of plate at 5X showing antigen specific B cells with signature
 352 reaction-diffusion pattern. Before and after 20X false color images of automated capture of an S1-RBD specific plasma cell. Blue indicates antigen
 353 beads displaying S1 RBD protein, while green indicates beads displaying S2 protein. Magenta is a cell specific stain. B) Example output from a
 354 SingleCyte Screen. For each cell, the confidence of an antigen specific interaction is determined by the amount of secondary antibody signal that
 355 overlaps an antigen-specific bead image in the proximity of each cell. A score of 0 represents a 50% chance of antigen specificity, with 1.0
 356 representing a 100% certainty.

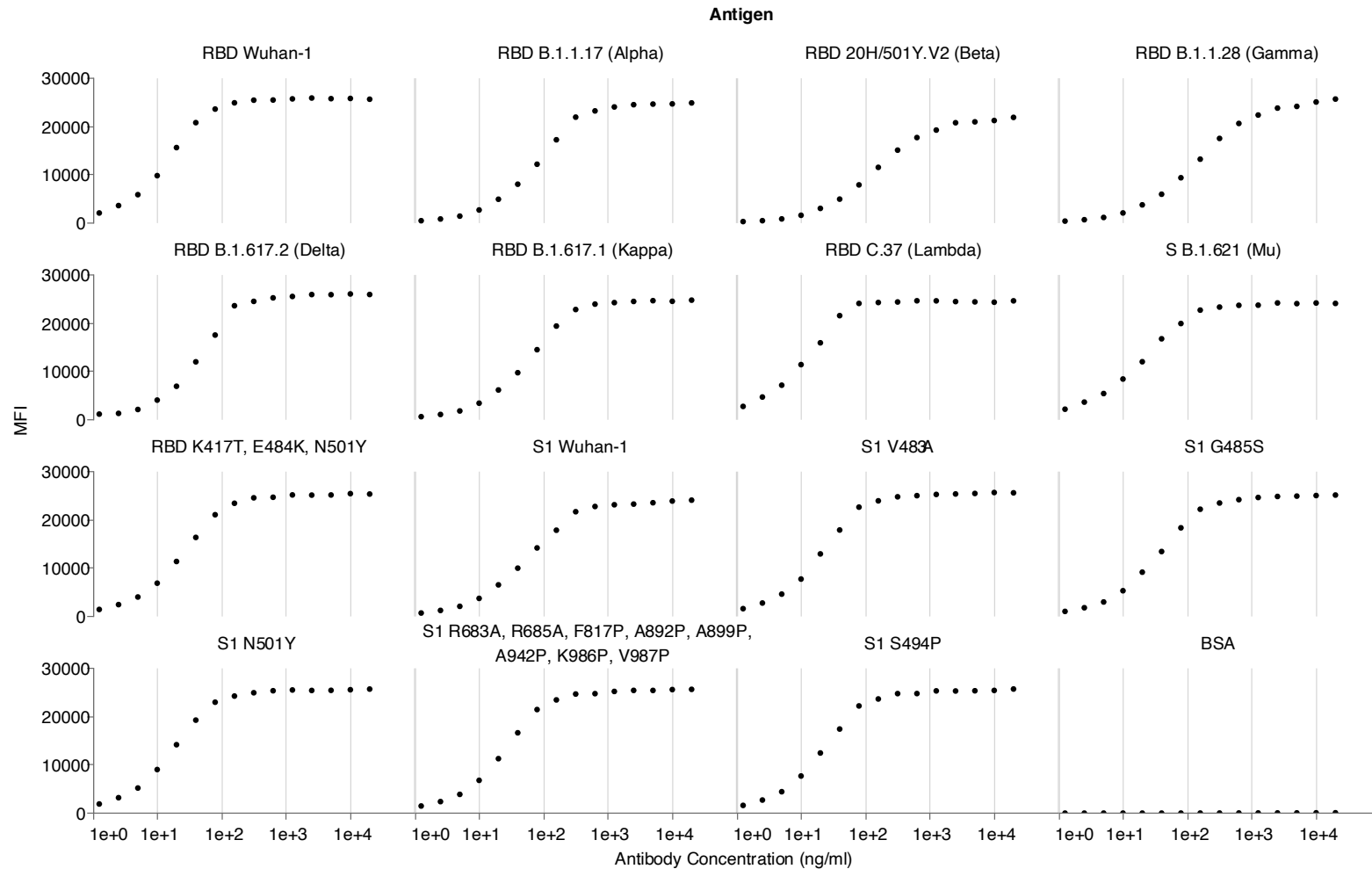


357

358 **Figure 3. Single domain affinity of AUG-3387 binding domain expressed as an ScFv.** The Catterra LSA platform was used to measure affinity of the
359 single chain version of AUG-3378 by flowing increasing concentrations of SARS-CoV-2 spike protein and measuring binding by surface plasmon
360 resonance.

361 **3.2.2 AUG-3387 Variant Binding Assays**

362 To assess the susceptibility of AUG-3387 to mutational escape, we profiled AUG-3387 against the
363 S1 and RBD portions of the original Wuhan-1 strain of SARS-CoV-2, RBD's corresponding to WHO
364 designated dominant strains of concern, and S1 mutants known to affect the potency of currently
365 approved therapeutic antibodies. AUG-3387 binds every S1 and RBD of SARS-CoV-2 tested with a
366 binding $EC_{50} < 200 \text{ ng/ml}$ (Figure 4), but only very weakly to SARS-CoV-1 (binding $EC_{50} > 100 \text{ ug/ml}$,
367 not shown). These data demonstrate the high potential for resistance to mutational escape of AUG-
368 3387.

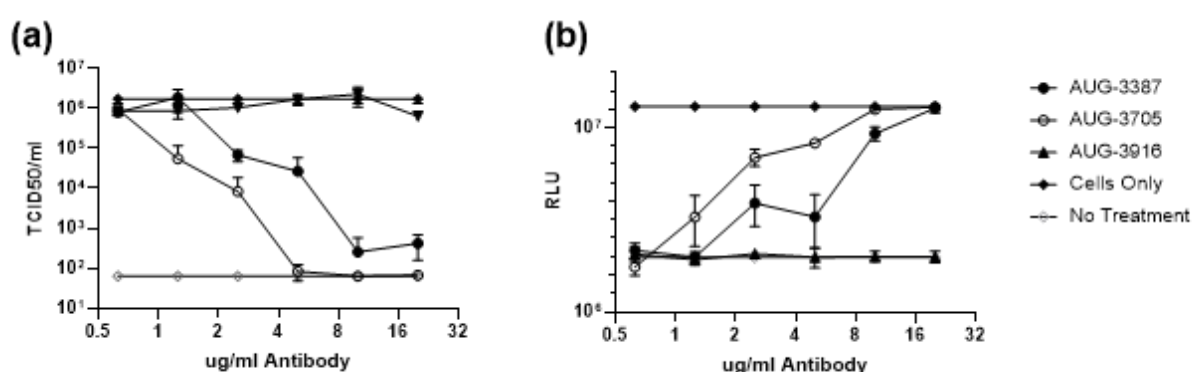


369

370 **Figure 4: illustrates the Resistance of AUG-3387 to Mutational Escape.** AUG-3387 was profiled against the S1 and RBD portions of the original
 371 Wuhan-1 strain of SARS-CoV-2, RBD's corresponding to WHO designated dominant strains of concern, and S1 mutants known to affect the potency
 372 of currently approved therapeutic antibodies. AUG-3387 binds every S1 and RBD of SARS-CoV-2 tested with a binding $EC_{50} < 200$ ng/ml, but only
 373 very weakly to SARS-CoV-1 (binding $EC_{50} > 100$ ug/ml, not shown).

374 3.2.3 AUG-3387 Neutralization of SARS-CoV-2 Wuhan-1

375 We compared the ability of full length IgG1 formatted AUG-3387 and its ScFv formatted version,
376 AUG-3705, to neutralize live SARS-CoV-2 in a 24 hour TCID50 assay and a 96 hour infected cell
377 viability assay (Figure 5). AUG-3705 demonstrated somewhat higher efficacy in these assays over
378 AUG-3387, indicating the improved avidity of the dimeric IgG1 did not improve neutralization
379 enough to compensate for the higher molarity of AUG-3705 at the same concentration.



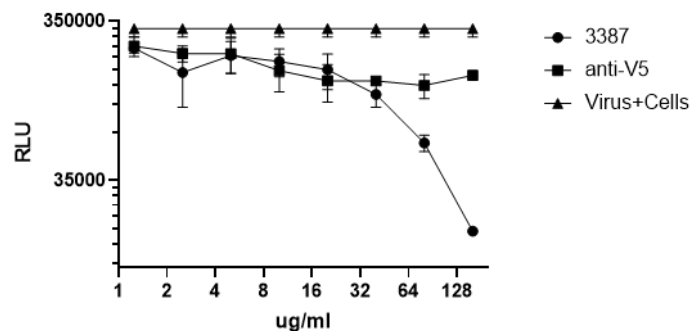
380

381 **Figure 5. Neutralization of SARS-CoV-2 by AUG-3387 and AUG-3705.** Neutralization was
382 determined by measuring TCID50 24 hours post infection (a) and measuring for viable cells
383 (CellTiterGlo luminescence) 96 hours post infection (b). In both assays, the dose-response curves
384 indicate an IC50 of ~2ug/ml or less.

385 3.2.3 AUG-3387 Neutralization of Delta Pseudovirus

386 We assessed the ability of AUG-3387 to neutralize the SARS-CoV-2 Delta variant pseudotyped virus
387 (Figure 6). AUG-3387 demonstrated the ability to neutralize Delta pseudovirus, although at a higher
388 IC50 (30-40 mg/mL) than for the Wuhan-1 strain (approximately 2 mg/mL in TCID50 assay).
389 However, the 30-40 mg/mL is still a clinically relevant dose that can be achieved by delivery to the
390 lung.

391



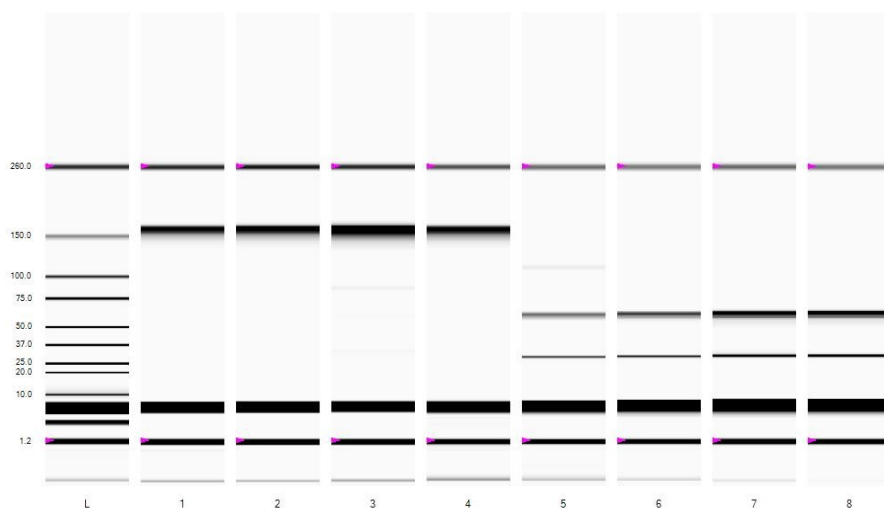
392

393 **Figure 6. Neutralization of SARS-CoV-2 B.1.617.2 (Delta) pseudovirus by AUG-3387.** Neutralization
394 was determined by measuring luciferase activity of cells infected with Delta pseudovirus after
395 treatment with AUG-3387.

396 3.3. TFF Powder Optimization and Characterization

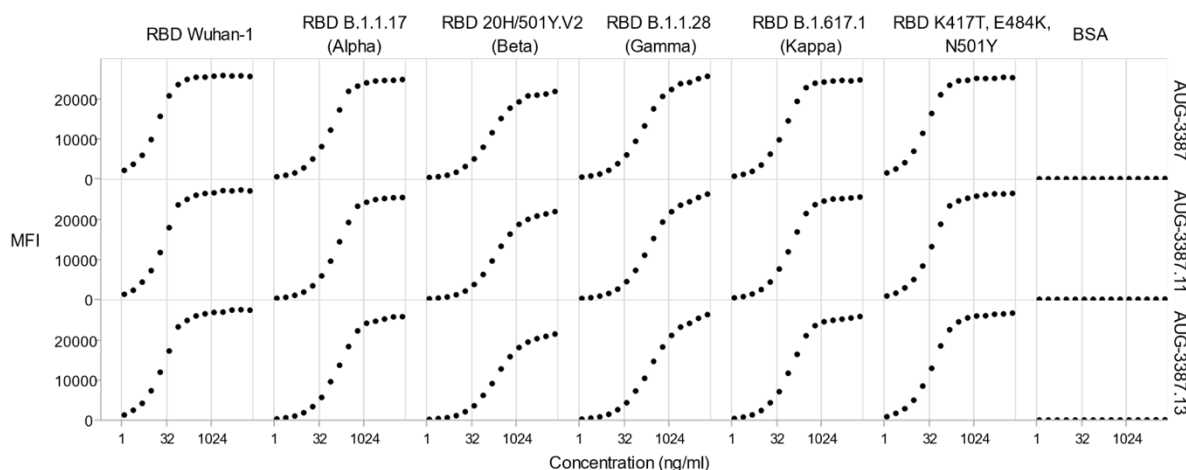
397 A series of dry powder formulations of AUG-3387 were prepared by Thin-Film Freezing and
398 evaluated for retention of biological activity and optimal aerosol properties for delivery to the lung.
399 The powders contained AUG-3387 at a range of mAb concentrations from 5-20% (w/w) and various
400 excipients. The powders were tested for the presences or absence of subvisible aggregates under a
401 light microscope, for mAb aggregation or fragmentation using SDS-PAGE, and for their aerosol
402 properties using the NGI. We assessed two formulations of AUG-3387 in TFF powders, AUG-3387.11
403 prepared with mannitol/leucine (95%/5%) and AUG-3387.13 prepared with trehalose/leucine
404 (95%/5%), and compared them to the original AUG-3387 formulation in PBS. AUG-3387.11 and
405 AUG-3387.13 performed virtually identically to their soluble counterpart in gel electrophoresis
406 (Figure 7A), multiplexed bead assays (Figure 7B).

407 **A)**



408

409 **B)**

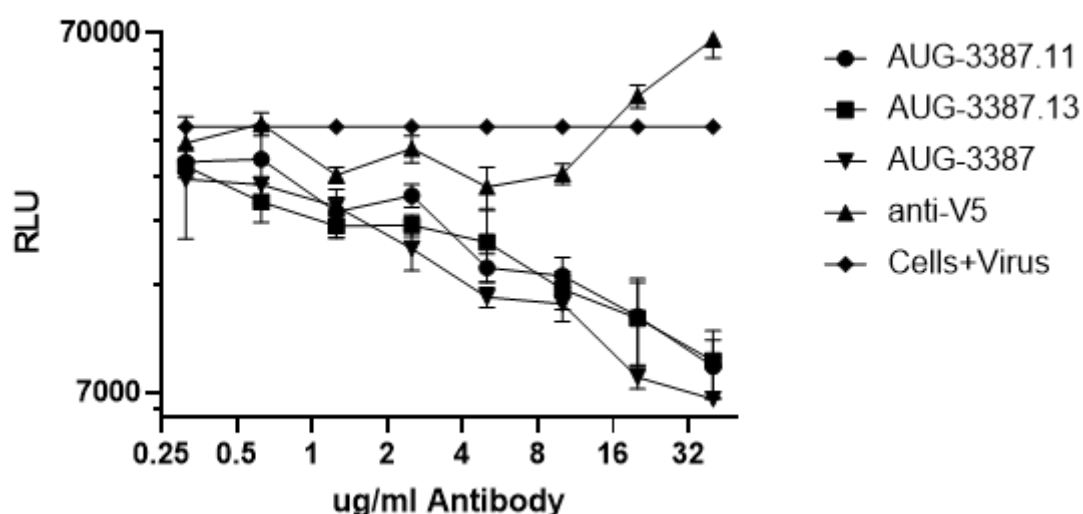


410

411 **Figure 7. Characterization of Dry Powder Formulations of AUG-3387 Prepared by Thin Film**
412 **Freezing.** A) Samples were run on a Bio-Rad Experion with AUG-3387.11 and AUG-3387.13 native in
413 lanes 1 and 2, reducing in lanes 5 and 6, respectively. AUG-3387 input mAb as expressed in Expi-
414 293T in lane 3 and 7 and CHO in lane 4 and 8. B) AUG-3387.11 and AUG-3387.13 bind to SARS-CoV-
415 2 variants at the same concentrations as the PBS formulation indicating that no loss of binding
416 occurred after the TFF processing to create dry powder formulations.

417 After verification that the dry powder formulations demonstrated no loss of binding activity, a
418 pseudoneutralization assay was used to confirm that the biological activity was retained. The dry
419 powder formulations were dissolved in media and added to the pseudoneutralization assay along
420 with the input antibody. Both dry powder formulations, AUG-3387.11 and AUG-3387.13, retained
421 full neutralization activity of the parental mAb (Figure 8).

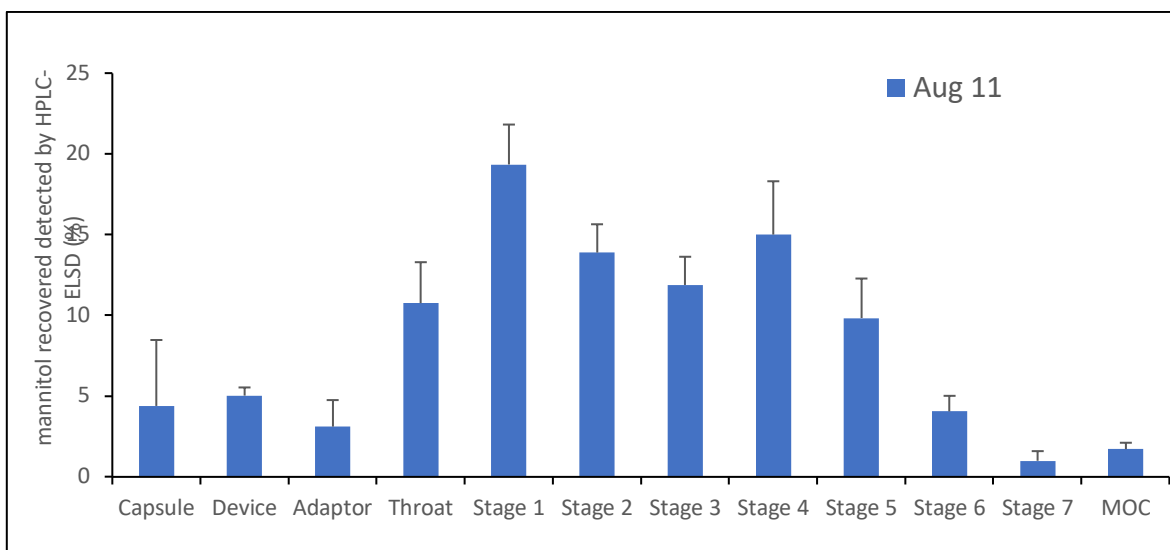
422



423

424 **Figure 8. Pseudoneutralization activity of Dry Powder Formulated AUG-3387.** and dry powder
425 formulations AUG-3387.11 and AUG-3387.13 demonstrate neutralization of SARS-CoV-2 Wuhan-1
426 pseudovirus at the same concentration as the PBS formulation

427 Final selection of the AUG-3387 dry powder formulation for *in vivo* characterization was complete
428 by evaluating the aerosol properties of the powders. The dry powder designated AUG-3387.11
429 showed excellent aerosol properties (Figure 9). This powder, delivered through a Plastiaple RS00 Dry
430 powder inhaler, gave an MMAD value of $3.74 \pm 0.73 \mu\text{m}$, a GSD of 2.73 ± 0.20 , and an FPF (delivered)
431 of $50.95 \pm 7.69\%$. Upon reconstitution of the powder, no significant subvisible aggregated particles
432 in the solution were observed under a microscope.



433

434

435

436

437

Figure 9. NGI Characterization of AUG-3387.11. Aerodynamic particle size distribution of AUG-3387.11 was determined by actuating a capsule for delivery using RS00 high-resistance DPI at a flow rate of 60 L/min (n =3) and quantitation of the powder on each stage of the impactor using an HPLC-ELSD method.

438

439

3.4. AUG-3387 Reduces SARS-CoV-2 Viral Load in Syrian Golden Hamsters

440

The efficacy of AUG-3387 for therapeutic reduction of viral load was assessed *in vivo* using the

441

established hamster model with the mAb formulations being delivered starting 24 hours after

442

intranasal SARS-CoV-2 inoculation. Hamsters were administered AUG-3387 at doses of 3 and 10

443

mg/kg or a vehicle control by intraperitoneal (IP) injection. Additional groups received three doses

444

of the TFF dry powder formulation of AUG-3387 by intratracheal (IT) instillation of at doses of 0.3

445

and 1 mg/kg at 24, 48, and 72 hours after SARS-CoV-2 inoculation. All animals showed body weight

446

loss. On Day 5, animals were harvested and lung tissues were assessed for viral replication by rt-

447

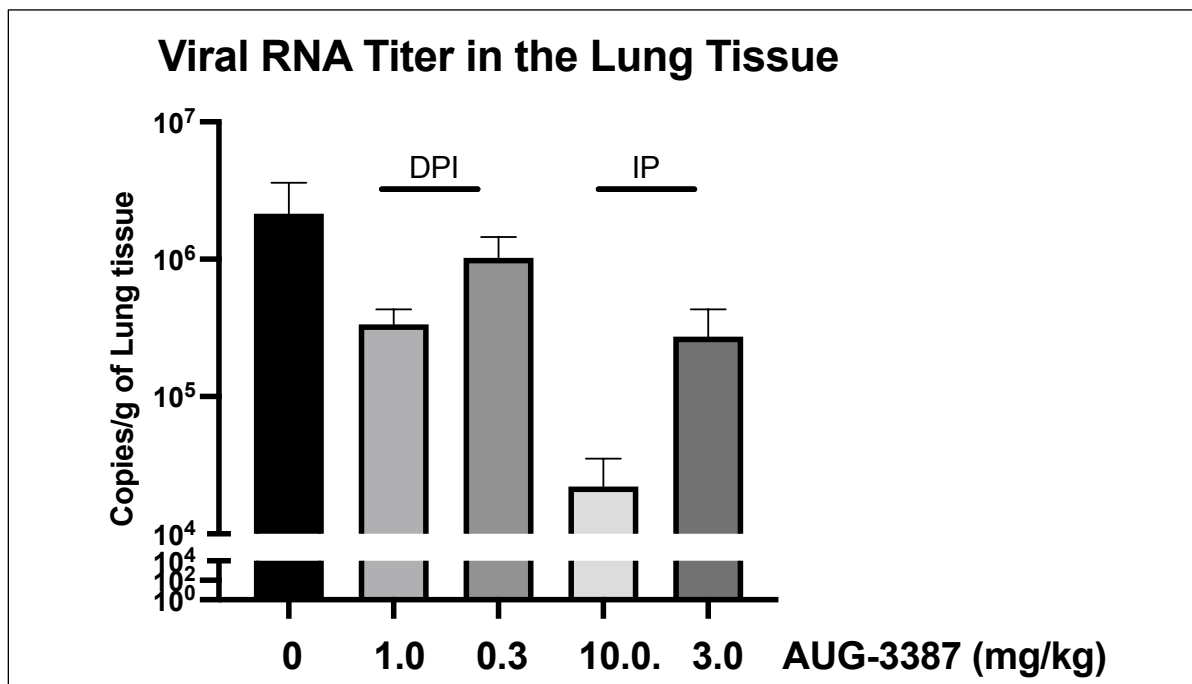
qPCR for subgenomic (active) viral replication. Dose dependent viral load reductions were observed

448

with both the IP and IT treated animals showing reduced viral load in the lung tissue, despite

449

treatment not being initiated until 24 hours after intranasal SARS-CoV-2 inoculation.



450 **Figure 10. Viral Load of SARS-CoV-2 Virus in Hamster Lung Tissue.** Following inoculation with
451 SARS-CoV-2 at time 0, treatment was initiated 24 hr later and animals were euthanized on Day 5.
452 Lung tissue was homogenized and active viral load was characterized by RT-qPCR for the E-gene.

453 4. Discussion

454 Since the start of the COVID-19 disease pandemic caused by the SARS-CoV-2, a high burden has
455 been placed on the healthcare system to provide adequate care and treatment of the high number
456 of patients infected by the virus that require hospitalization. Patient care has improved as the
457 pandemic has progressed and the mortality rate has dropped as the care has improved. One key
458 area of improvement in patient outcomes occurred when anti-SARS-CoV-2 monoclonal antibody
459 therapies became available. While not highly efficacious for the treatment of severe COVID-19
460 disease, the current mAb therapies demonstrate up to a 79% reduction in hospitalization in patients
461 that are symptomatic and at high risk to develop severe disease that will require hospitalization.
462 These risk factors include age greater than 65 years, obesity or being overweight, pregnancy,
463 diabetes, chronic kidney disease, immunocompromised patients due to disease or
464 immunosuppressive treatment, cardiovascular disease, chronic lung diseases or sickle cell disease.

465 In these patients, mAb therapy has been demonstrated to reduce hospitalization by up to nearly
466 80% when administered early in the course of disease when the patients present with mild to
467 moderate disease.

468 However, each of the mAb products currently authorized under EUA by the FDA are administered
469 by intravenous infusion, which requires the patient of have the infusion performed in a healthcare
470 setting where infusion personnel are adequately trained to perform intravenous catheter placement
471 and administration of the IV solutions. While these mAb therapeutics provide a clear therapeutic
472 benefit for the reduction of hospitalization, the route of administration continues to place a burden
473 on the healthcare system to deliver these therapies to the patients and their families. Thus, delivery
474 of mAb therapy to patients in an outpatient setting without the need for specialized infusion centers
475 would provide a clear advancement. Furthermore, since only a fraction of systemically administered
476 antibodies reaches the lung from systemic administration, localized delivery to the lung would
477 represent an advantage over intravenous delivery because the virus replicates in the pulmonary
478 epithelial cells early in the infection and can be administered at lower total doses per patient.

479 The SingleCyte® system was used to isolate a new mAb, designated AUG-3387, that displays potent
480 binding to the SARS-CoV-2 S-protein. Binding to and neutralization of both pseudovirus and Wuhan-
481 1 Coronavirus demonstrated the potential utility of AUG-3387 for treatment of COVID-19 disease.
482 AUG-3387 demonstrated potent binding to the Alpha, Beta, Gamma, Delta, Lamda and Mu variants
483 suggesting that AUG-3387 binds a conserved epitope that has not mutated in the variants of concern
484 or newly emerging Lamda and Mu variants. Furthermore, neutralization and pseudoneutralization
485 data demonstrate that AUG-3387 prevents the virus from infecting cells by blocking interaction of
486 this conserved region of the RBD with the hACE2 receptor of target cells. The retained activity
487 against all tested variants is in contrast to the reduced susceptibility of Bamlanivimab and

488 Etesevimab, which show greater than 250-fold reduced binding and neutralization activity against
489 the Beta and Gamma variants (16).

490 In order to differentiate AUG-3387 from the current mAb therapeutics that are currently being used
491 under EUA, the mAb has been formulated as a room temperature stable dry powder utilizing the
492 thin-film freezing process. The room temperature stability may allow for distribution to geographic
493 locations where SARS-CoV-2 continues to spread but that do not have the capability of distributing
494 injectible formulations that require cold chain distribution and storage. We demonstrated that the
495 formulations prepared using the TFF process retain full binding activity of the input mAb solutions
496 and have no evidence of protein aggregation or instability following reconstitution in water.

497 In addition to the dry powder storage at room temperature of the TFF formulated dry powder mAb,
498 the dry powders can be encapsulated and delivered to the lung using a standard dry powder inhaler
499 device. When tested with the Plastiaple RS00 high resistance device, which is designed to provide
500 maximum shear and aerosolization of powders at lower airflow rates, the AUG-3387 powder
501 formulations had a fine particle fraction with greater than 50% of the powder in the 1-5 μm range,
502 which is ideal for delivery to the deep lung of humans using a device matched to the potential for
503 reduced lung function for mild to moderate COVID-19 patients.

504 Finally, we demonstrated that administration of AUG-3387 by either intraperitoneal injection or by
505 intratracheal insufflation of the dry powder into SARS-CoV-2 infected Syrian hamsters resulted in a
506 dose dependent reduction of the viral load in the lung tissue of the infected hamsters. The result
507 of this *in vivo* study is notable because we utilized a treatment paradigm that creates a high burden
508 for efficacy to be demonstrated. In our study, mAb treatment of the hamsters was not initiated until
509 24 hours after the hamsters were infected with SARS-CoV-2 by intranasal inoculation. By contrast,
510 sotrovimab administered by IP injection prophylactically at doses of 5 mg/kg or more when given

511 24- or 48-hours prior to viral infection resulted in improvement in body weight loss and decreased
512 viral load in the lung tissue compared to control animals. Likewise, the casirivimab and imdevimab
513 combination of mAbs administered to hamsters by IP injection 24 hours before viral inoculation (17)
514 resulted in a dose dependent viral load reduction in lung tissue. However, no change in viral load in
515 the lung tissue was reported when casirivimab and imdevimab were administered 24 hours after
516 viral inoculation in a manner similar to our study. For sotrovimab there was no report of therapeutic
517 treatment resulting in reduced viral load. Thus, to date, the demonstration that AUG-3387
518 administered by either IP or IT routes in a therapeutic mode resulted in a dose dependent viral load
519 reduction in the lung tissue represents the first report of a mAb therapy that works in the hamster
520 model in a therapeutic mode. Furthermore, the viral load reduction of the dry powder when
521 delivered by IT insufflation represents the first report of successful reduction of viral load using
522 inhaled delivery of a mAb therapeutic for COVID-19 disease.

523 Taken together, these data suggest that AUG-3387 is a potent mAb that has the potential to treat
524 all known variants of SARS-CoV-2 and that the powders produced by the TFF formulation process to
525 make room temperature stable powders has the potential to reduce the amount of mAb needed for
526 efficacy because of the local delivery to the lung. Furthermore, since the TFF AUG-3387 powder
527 does not require cold chain storage, it represents an opportunity to distribute the powder
528 formulation globally to reduce the human cost of the COVID-19 pandemic by facilitating delivery of
529 this therapy to locations lacking cold chain distribution capabilities.

530

531 **Acknowledgements:** The authors would like to thank the laboratory of Peter S. Kim for sharing
532 trimeric SARS-CoV1/2 spike proteins and performing preliminary pseudoneutralization assays, Sarah
533 A. Stanley for access to BSL3 facilities at UC Berkeley, and Daniel Bedinger of Carterra LSA for
534 determining affinity of AUG-3705 and other Augmenta antibodies. We also greatly appreciate the
535 contributions to Augmenta's platform and discovery efforts by Payam Shahi, John Beaber, Rosanna
536 Chau, Cindy Y. Lai, Kim X. Nguyen, Robin Emig, John R. Haliburton, Max Von Franque, Niklas
537 Mannhardt, Isaac Perper, Micah Kelly, Sarah Galloway, Rachel Brewer, Paige Hansen, Jeremiah
538 Budiman, Helen Chang, and William Horvat.

539 **Funding:** This research was funded by TFF Pharmaceuticals and Augmenta Bioworks. Williams and
540 Cui were supported by a sponsored research agreement and a technology validation agreement
541 from TFF Pharmaceuticals, Inc. Fox and Nguyenla were supported by a Mercatus Center Fast Grant.

542 **Conflicts of Interest:** Cui reports financial support was provided by TFF Pharmaceuticals. Cui
543 reports a relationship with TFF Pharmaceuticals, Inc. that includes: equity or stocks and funding
544 grants. Williams reports a relationship with TFF Pharmaceuticals, Inc. that includes: consulting or
545 advisory, equity or stocks, and funding grants. Xu, Moon and Sahakijpijarn report a relationship
546 with TFF Pharmaceuticals, Inc. that includes: consulting or advisory. Christensen is a consultant for
547 TFF Pharmaceuticals.

548 Emig, Mena, Vitug, Henry, and Ventura are or were employees of Augmenta Bioworks, Inc.

549 Emig, Mena, Vitug, Henry, Cui, Xu, Williams, and Christensen are inventors on IP related to

550 this work.

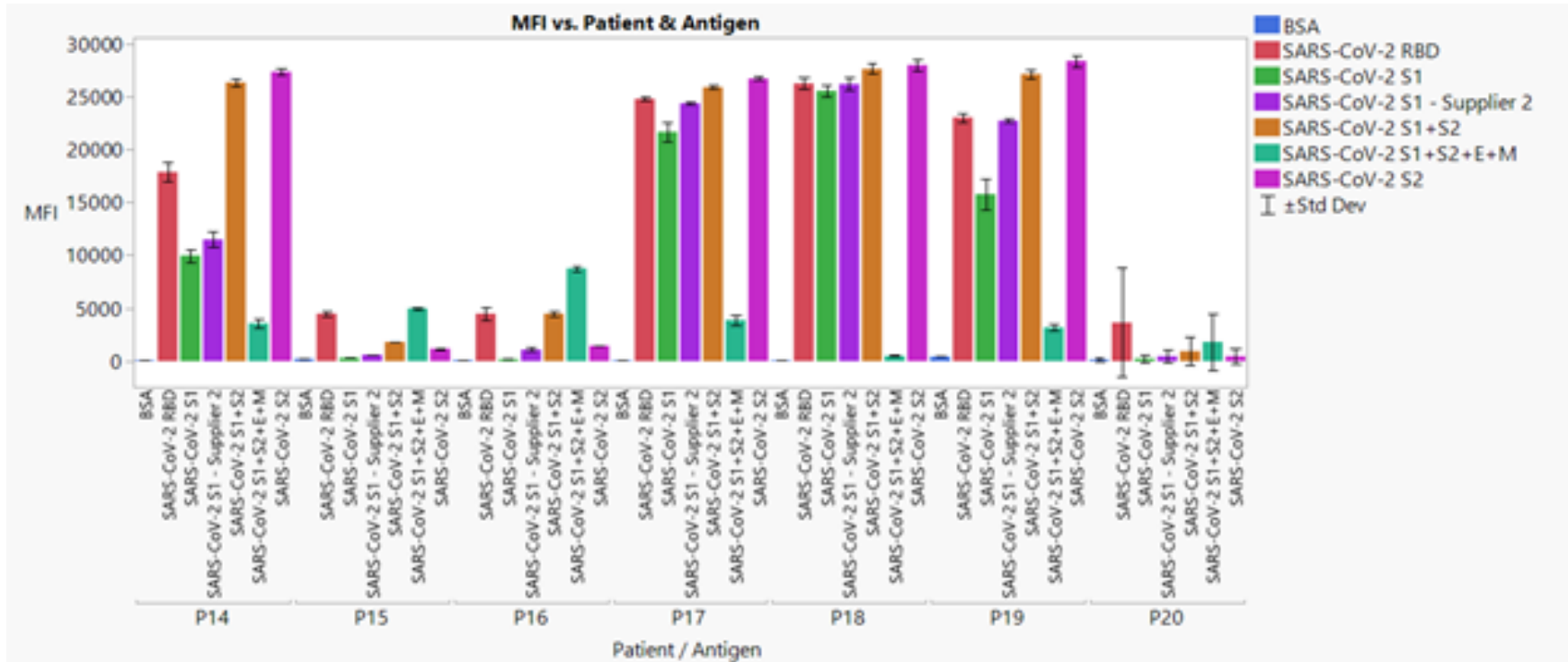
551 **References**

552

- 553 1. K. Miller, M. E. McGrath, Z. Hu, S. Ariannejad, S. Weston, M. Frieman, W. T. Jackson,
554 Coronavirus interactions with the cellular autophagy machinery. *Autophagy* **16**, 2131-2139
555 (2020).
- 556 2. F. Wu, S. Zhao, B. Yu, Y.-M. Chen, W. Wang, Z.-G. Song, Y. Hu, Z.-W. Tao, J.-H. Tian, Y.-Y.
557 Pei, A new coronavirus associated with human respiratory disease in China. *Nature* **579**,
558 265-269 (2020).
- 559 3. D. Gurwitz, Angiotensin receptor blockers as tentative SARS-CoV-2 therapeutics. *Drug*
560 *development research* **81**, 537-540 (2020).
- 561 4. G. Xue, X. Gan, Z. Wu, D. Xie, Y. Xiong, L. Hua, B. Zhou, N. Zhou, J. Xiang, J. Li, Novel
562 serological biomarkers for inflammation in predicting disease severity in patients with
563 COVID-19. *International immunopharmacology* **89**, 107065 (2020).
- 564 5. H.-X. Liao, M. C. Levesque, A. Nagel, A. Dixon, R. Zhang, E. Walter, R. Parks, J. Whitesides,
565 D. J. Marshall, K.-K. Hwang, High-throughput isolation of immunoglobulin genes from
566 single human B cells and expression as monoclonal antibodies. *Journal of virological*
567 *methods* **158**, 171-179 (2009).
- 568 6. T. Tiller, E. Meffre, S. Yurasov, M. Tsuiji, M. C. Nussenzweig, H. Wardemann, Efficient
569 generation of monoclonal antibodies from single human B cells by single cell RT-PCR and
570 expression vector cloning. *Journal of immunological methods* **329**, 112-124 (2008).
- 571 7. J. Wrammert, K. Smith, J. Miller, W. A. Langley, K. Kokko, C. Larsen, N.-Y. Zheng, I. Mays, L.
572 Garman, C. Helms, Rapid cloning of high-affinity human monoclonal antibodies against
573 influenza virus. *Nature* **453**, 667-671 (2008).
- 574 8. U.S. National Library of Medicine. (2021, May 6). Identifier NCT04872231, Single
575 Ascending Dose and Multiple Ascending Dose Study of Voriconazole Inhalation Powder in
576 Healthy Adult Subjects. *Clinicaltrials.Gov*. <https://clinicaltrials.gov/ct2/show/NCT04872231>
- 577 9. U.S. National Library of Medicine. (2021, October 6). Identifier NCT04576325,
578 Pharmacokinetic Profile of Voriconazole Inhalation Powder in Adult Subjects With Asthma.
579 *Clinicaltrials.Gov*. <https://clinicaltrials.gov/ct2/show/NCT04576325>
- 580 10. N. A. Beinborn, J. Du, N. P. Wiederhold, H. D. Smyth, R. O. Williams, 3rd, Dry powder
581 insufflation of crystalline and amorphous voriconazole formulations produced by thin film
582 freezing to mice. *Eur J Pharm Biopharm* **81**, 600-608 (2012).
- 583 11. C. Moon, S. Sahakijpiparn, J. J. Koleng, R. O. Williams, Processing design space is critical for
584 voriconazole nanoaggregates for dry powder inhalation produced by thin film freezing.
585 *Journal of Drug Delivery Science and Technology* **54**, (2019).
- 586 12. C. Moon, A. B. Watts, X. Lu, Y. Su, R. O. Williams, 3rd, Enhanced Aerosolization of High
587 Potency Nanoaggregates of Voriconazole by Dry Powder Inhalation. *Mol Pharm* **16**, 1799-
588 1812 (2019).
- 589 13. S. Sahakijpiparn, C. Moon, X. Ma, Y. Su, J. J. Koleng, A. Dolocan, R. O. Williams, 3rd, Using
590 thin film freezing to minimize excipients in inhalable tacrolimus dry powder formulations.
591 *Int J Pharm* **586**, 119490 (2020).
- 592 14. S. Hufnagel, S. Sahakijpiparn, C. Moon, Z. Cui, R. O. Williams III, The Development of Thin-
593 film Freezing and Its Application to Improve Delivery of Biologics as Dry Powder Aerosols.
594 *KONA Powder and Particle Journal*, 2022010 (2022).
- 595 15. L. J. Reed, H. Muench, A simple method of estimating fifty per cent endpoints. *American*
596 *journal of epidemiology* **27**, 493-497 (1938).

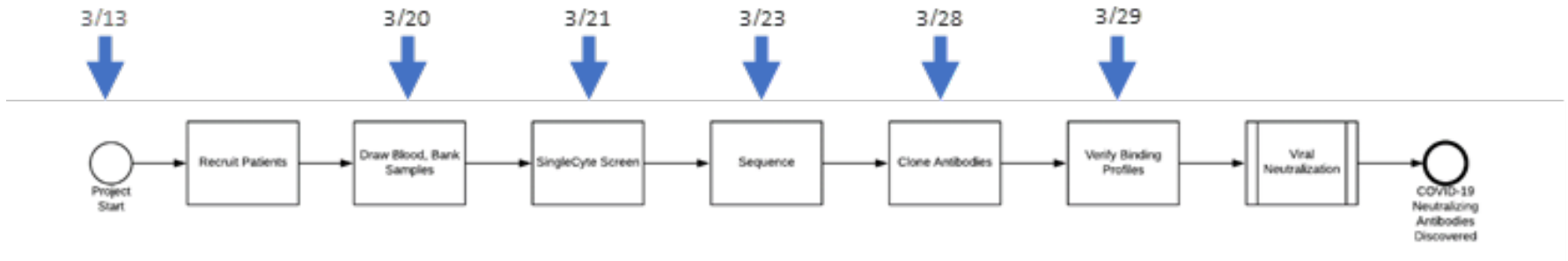
- 597 16. Fact sheet for health care providers emergency use authorization (EUA) of bamlanivimab
598 and etesevimab. (2021, September 16). *U.S. FDA*.
599 <https://www.fda.gov/media/145802/download>
600 17. A. Baum, D. Ajithdoss, R. Copin, A. Zhou, K. Lanza, N. Negron, M. Ni, Y. Wei, K.
601 Mohammadi, B. Musser, REGN-COV2 antibodies prevent and treat SARS-CoV-2 infection in
602 rhesus macaques and hamsters. *Science* **370**, 1110-1115 (2020).
603

604



605

606 **Supplemental Figure 1. Serological profile of 7 patients against 6 SARS-CoV-2 antigens generated by diluting plasma 1:1000 in a 6 plex Luminex assay.**
607 Samples from each patient were evaluated for binding to antigen proteins including the Receptor binding domain (RBD), Spike Protein 1 (S1), Spike Protein 2
608 (S2), the E-protein (E), and M protein (M) coated on Luminex beads.



609

610

611

612

Supplemental Figure 2. Timeline for discovery of Augmenta's first SARS-CoV-2 antibodies.